NOTES AND CORRESPONDENCE

Spectral Tail of a Gravity Wave Train Propagating in a Shearing Background

MANUEL PULIDO AND GIORGIO CARANTI

*Grupo de Física de la Atmósfera, Facultad de Matemática Astronomia y Física, Universidad Nacional de Córdoba,
Ciudad Universitaria, Cordoba, Argentina*

ABSTRACT

The causes of the appearance of a tail in the power spectrum of a gravity wave train in a shearing background terminating under the Hodges condition are studied. The power spectrum of this train for a wavenumber greater than the cutoff value has amplitudes and slopes similar to the observed in actual wind profiles. It is shown that the Fourier transform for large wavenumbers can be expressed as an inverse power series of the wavenumber, where the first two terms are dominant (k^{-1} and k^{-2}) with a power spectrum slope from -2 to -4 in the tail. The main features that produce the tail are the discontinuities in the profile.

An observed profile is analyzed showing that the power spectral amplitudes do not necessarily come from the waves contained in the profile; they can arise from irregularities, nonperiodic jumps that could be interpreted as discontinuities.

1. Introduction

The power spectrum (PS) of horizontal winds and temperatures along vertical profiles in very different geographical locations and height ranges present some sort of universal behavior. First reported by VanZandt (1982), these results and subsequent works suggest that the slopes of the spectra are in a range from -3.1 to -2.4 (Allen and Vincent 1995). With the purpose of explaining this spectral shape a number of theoretical works were carried out. These works can be classified into three categories: 1) saturation models (Dewan and Good 1986), which involve saturated waves caused by convective and shear instability limiting the exponential growth; 2) Doppler spread (Hines 1991) where the tail is a consequence of Doppler spreading by background winds generated by the wave system itself; and 3) diffusive models (Weinstock 1990) in which there are interactions among waves through diffusive processes.

There are works that associate the spectral tail to terminating waves; Sato and Yamada (1994) showed that the spectrum of one terminating wave, with saturation amplitude, has a slope of -4 for internal waves and of -3 for inertial waves. Recently, Chimonas (1997) proposed a new model to simulate wind irregularities using a train of quasi-random gravity shear waves (gravity waves propagating in a shearing background). This results in a wind profile perturbation giving a PS tail with appropriate slopes and amplitudes. The profile so constructed shows similarities with measured profiles. Reanalyzing the data, Chimonas observes that the real spectrum terminates at a cutoff wavenumber, m_*, where the overturning starts ($N^2 = 0$; Hodges 1967). Further, he observes that the profiles, when Fourier transformed, present a high wavenumber tail with slope -2.7 and claims that this tail is an artifact of the transformation. The wave terminations determine the slope of the spectral tail.

The objective of this note is to present a study of the spectral tail of a Fourier-transformed train of gravity shear waves and to give an explanation for the slope values. It is concluded that the tail is an effect of the Fourier transform since the tail contains wavenumbers larger than the actual cutoff of the waves. If discontinuities in the profile or in any of its derivatives are present, there will be a spectral tail formation. This effect calls to mind a similar one known as ''leakage,'' first noted in spectra of signals abruptly terminated at the end of the sampling interval (Brigham 1974; Press et al. 1992). We will find an expansion in inverse powers of the wavenumber for wavenumbers larger than the cutoff value, showing that with only the first few terms of this expansion the tail is formed and the slopes lie in the -4 to -2 range.

In section 5 we show that this ''contamination'' effect is present in real profiles when they are Fourier trans-

Corresponding author address: Dr. Manuel Pulido, Facultad de Matemática Astronomia y Fisica, Universidad Nacional de Córdoba, Ciudad Universitaria, (5000) Cordoba, Argentina.
E-mail: pulido@roble.fis.uncor.edu

formed. Abrupt changes in the wind perturbation generate spectral amplitudes in high wavenumbers.

2. The model

The model we used is similar to Chimonas (1997). A simplified description of it is given below, and the reader will find more details in his work. Let us assume a gravity wave propagating in an inviscid fluid with $\lambda_x \gg \lambda$, where λ_x and λ are the horizontal and the vertical wavelengths, respectively. The use of the plane defined by the propagation direction and the vertical simplifies the treatment.

The corresponding dispersion relation is

$$k = \frac{N}{c - U(z)}, \quad (2.1)$$

with $k = 2\pi/\lambda$, and N is the Brünt-Väisälä frequency mean, c is the horizontal phase speed, and $U(z)$ is the background wind. In order to avoid the frequent use of the factor 2π, we will also use $m = 1/\lambda$, in cycles per meter, instead of k.

The background wind velocity is given, in a range of altitudes, by

$$U = c + (z - z_c)U'(z_c), \quad (2.2)$$

where z_c is the altitude of the critical level.

From the linearized equations, the solution for the perturbation of the vertical velocity will be (e.g., Teitelbaum and Sidi 1979)

$$w(x, z, t) = A\rho_0^{1/2}(z - z_c)^{(1/2)\pm i\mu} \exp[ik_x(ct - x)], \quad (2.3)$$

where $\mu = \sqrt{\text{Ri} - \frac{1}{4}}$ and Ri is the Richardson number for the background [$\text{Ri} = N^2/U'(z_c)$]. The horizontal component of the perturbation is

$$u = -\frac{i}{k_x}\frac{\partial w}{\partial z}. \quad (2.4)$$

In the neighborhood of the critical level, the density changes with altitude can be ignored; then

$$u(z) = B(z - z_c)^{-1/2} \exp\{\pm i\mu \log[C(z - z_c)]\}. \quad (2.5)$$

Since the wave will end somewhere between the Hodges (1967) condition level and the critical level, Chimonas suggested two possible cases: a sudden wave termination exactly at the Hodges condition and a relatively fast oscillating decay up to the critical level.

He found that the abrupt-termination case had a better correspondence with the spectra of measured profiles. Therefore, the equations used are [(A1) in Chimonas 1997]

$$u = \begin{cases} A\left(\dfrac{z_c - z_b}{z_c - z}\right)^{1/2} \cos\left(-\mu \log\left(\dfrac{z_c - z}{z_c - z_b}\right)\right) & z < z_b \\ 0 & z \geq z_b, \end{cases} \quad (2.6)$$

where z_b is the point where the Hodges condition ($N^2 = 0$) is fulfilled.

Assuming the existence of many sources, there will be a set of upward propagating waves with different phase velocities. Therefore each wave will correspond to a critical level height according to both its phase velocity and the mean wind profile.

Supposing that the phase velocity space is quantified in units of Δc, which are statistically independent, a superposition of waves is constructed where each Δc is associated with a terminating wave. Given the mean wind profile, there exists a correspondence between Δc and Δz, so one can interpret that each termination is associated with a height interval Δz.

Both the altitude of the critical level within the interval Δz and the wave amplitude between 0 and u_b are at random. Here, u_b is the saturation amplitude (Fritts 1984), given by

$$u(z_b) = |c - U(z_b)|. \quad (2.7)$$

Using the dispersion relation, the following expression for u_b is obtained:

$$u(z_b) = N/k_*, \quad (2.8)$$

where k_* is the highest wavenumber present in the train of waves.

The parameters are defined as in Chimonas (1997). Both the distance between the Hodges condition altitude and the critical level, and the interval Δz, are considered of the order of $1/m_*$, which is the scale of the problem. The mean Richardson number is taken as order of 10, which is characteristic of stratospheric levels.

3. Mathematical considerations

Let us assume a vertical profile $u(z)$ in the interval $[0, L]$. The coefficients of its Fourier transform are given by

$$C_n = \frac{1}{\sqrt{L}} \int_0^L u(z) \exp(-i2\pi nz/L) \, dz, \quad (3.1)$$

where n/L is the vertical wavenumber m.

If $u(z)$ has $N + 1$ discontinuities of any order (i.e., discontinuities in the function and/or any of its derivatives), the integrating interval can be divided in, say, N subintervals. Let us assume that the discontinuities are located at z_j, with $j = 0, \ldots, N$. Then the integral (3.1) will be expressed as a sum of integrals as follows:

$$C_n = \frac{1}{\sqrt{L}} \sum_{j=0}^{N-1} \int_{z_j}^{z_{j+1}} u(z) \exp(-i2\pi nz/L) \, dz, \quad (3.2)$$

where $z_0 = 0$ and $z_N = L$.

Since $u(z)$ is analytical in (z_j, z_{j+1}), we can integrate it by parts to get

$$D_n = -\frac{1}{\sqrt{L}} \sum_{j=0}^{N-1} \sum_{s=0}^{\infty} \frac{u^{(s)}(z)}{(ik)^{s+1}} \exp(-ikz)\Big|_{z_j^-}^{z_{j+1}^+}, \quad (3.3)$$
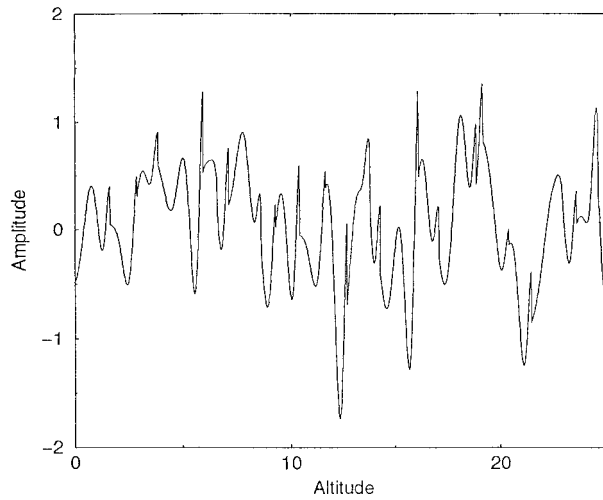
FIG. 1. Profile generated with the model. The superposition includes 30 propagating waves terminating abruptly. Altitudes are measured in units of $1/m_*$, which is of the order of 1 km in the stratosphere. Amplitudes are measured in units of N/k_*.
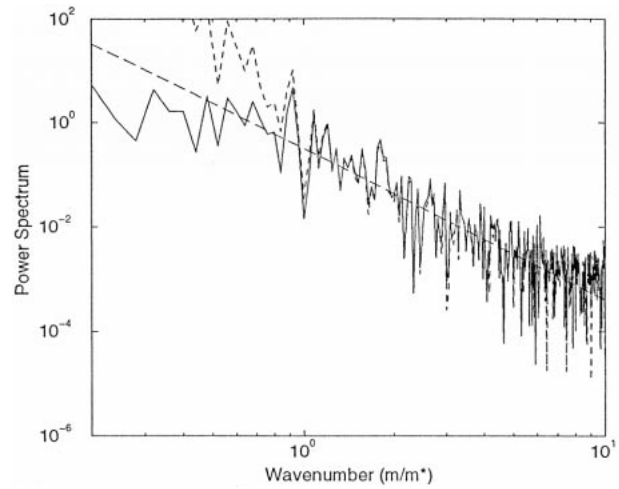

FIG. 2. Power spectrum for the profile of Fig. 1. The full line represents the power spectrum calculated with the Fourier transform; the dashed line represents the approximation to the power spectrum with the power series; and the straight line represents a fitting to the Fourier spectrum.

where $u^{(s)}(z_j^+)$ is the s derivative evaluated in z_j from the right, and $u^{(s)}(z_j^-)$ corresponds to the evaluation from the left. Thus the Fourier coefficients can be expanded in negative powers of k. The series, D_n, is convergent to the solution C_n for large enough k (Erdélyi 1956).

The s term in (3.3), written in terms of the discontinuities, will be

$$D_n^s = -\frac{1}{\sqrt{L}(ik)^{s+1}}\left[\sum_{j=1}^{N-1} \Delta^s u_j \exp(-ikz_j) + u^s(L) - u^s(0)\right],$$
(3.4)

where $\Delta^s u_j = u^{(s)}(z_j^+) - u^{(s)}(z_j^-)$.

The presence of discontinuities in the profile leads to the generation of amplitudes in high wavenumbers. From (3.3) the power spectrum will depend on inverse powers of k (k^{-n} with $n \geq 2$).

Discontinuities at the interval ends $[0, L]$ produce an effect called "leakage" (Brigham 1982), similar to the one described above. The leakage phenomenon is usually diminished by the use of windowing. It can be seen, for example, that the use of a triangular window changes the leakage from k^{-2} to k^{-4} because the discontinuity is now on the derivative. For the case of the wave train, since the discontinuities are inside the interval, the generated leakage will be called internal leakage.

4. Spectral analysis of the generated profiles

The model profiles (see section 2) have discontinuities in the $u(z)$ and successive derivatives in the points z_{bj}. The asymptotic expansion will be convergent to C_n (3.4) if

$$\left|\frac{D_n^s}{D_n^{s+1}}\right| = k\left|\frac{\sum_{j=1}^{N-1} \Delta^s u_j \exp(-ikz_j)}{\sum_{j=1}^{N-1} \Delta^{s+1} u_j \exp(-ikz_j)}\right| < 1.$$

Taking

$$\Delta^s u_j = \frac{\mu^s}{(z_{cj} - z_{bj})^s}$$

and $m_* = 1/(z_{cj} - z_{bj})$, the ratio of successive terms is

$$\left|\frac{D_n^s}{D_{s+1}^s}\right| = \frac{2\pi m}{\mu m_*}.$$

The first term will be the dominant one if $m > (\mu/2\pi)m_*$. Conversely, for $m < (\mu/2\pi)m_*$, for any s order, the terms are of the same order and an approximation with few terms will not be possible. This can be traced down to waves in the profile with that wavenumber m, as it can be seen in (3.4).

Simulations running the model were carried out; Fig. 1 shows a generated profile of $u(z)$. The power spectrum is then calculated using the Fourier transform and from the series expansion in inverse powers. A good approximation is obtained using the series up to $s = 3$ for $m > m_*$. In Fig. 2, the two PSs are compared. A least squares fitting was also included in the graph. The slopes obtained in the interval $[m_*, 8m_*]$ can be seen in Table 1. Figure 2 also shows the role that threshold m_* plays quite clearly. Above m_* the approximation closely matches effects generated by the Fourier transform, while below this threshold the PS and the approximation depart drastically due to the presence of genuine waves.

To verify the stability of the used approximation, 30

TABLE 1. Parameters from a least square fitting for the Fourier power spectrum (FT) and for the inverse power series (approx). Ordinates are given in $8(2\pi)^2 m_*^3 C_n^2/N^2$.

Type	Ordinate		Slope	
	FT	Approx	FT	Approx
Profile	0.317	0.283	−2.89	−2.90
Mean	0.726	0.693	−2.88	−2.91

profiles were simulated, and the resulting spectral mean together with the spectral mean from the inverse power series are shown in Fig. 3. There are only small differences, which one can ascribe to the discrete nature of the data. Supporting this fact, the results with a larger number of points show decreasing differences. Table 1 presents the results of fitting the mean PS with a least squares procedure.

Fittings of the mean PS suggest three regions: a small portion between m_* and $1.5m_*$ where the second and third term of the series are dominant with slope −4, a central region $(1.5m_* < m < 4m_*)$ where the first and second terms are dominant with slope close to −3, and a region for greater wavenumbers with slopes close to −2.

A shared characteristic between the power spectra of actual profiles and the present modeled results are the oscillations observed in the tail. The dispersion of the results arises from the discontinuities inside the interval, and while in other works this was assigned to spectral noise, Chimonas (1997) assigned it to the quasi-random nature of the spectra generated. In fact, from Eq. (3.3) it can be seen that the oscillations are related to the factors $\exp(-ikz)$. To show this, let us work out an example with only two discontinuities in the interval. Taking into account only the first-order terms in the expansion (3.3), the expression of the PS will be

$$|D_n|^2 = \frac{1}{Lk^2}\{\Delta u_1^2 + \Delta u_2^2 + 2\Delta u_1 \Delta u_2 \cos[k(z_2 - z_1)]\},$$

(4.1)

where Δu_1 and Δu_2 are the discontinuities in z_1 and z_2.

The oscillations in (4.1) have a ''wavelength'' in the k space that depends on the distance between discontinuities, from half a wavelength in the whole range of m (i.e., with $0 \le m \le m_c$ where m_c corresponds to the Nyquist frequency) to one wavelength every two harmonics.

5. Analysis of an observed profile

In the following analysis, data from a measured profile is used to show the existence of internal leakage. The data, covering the 1–9-km height range, comes from the Jimsphere technique (Endlich et al. 1969) and was taken in Cape Kennedy, Florida, on 16 April 1967.

The wind perturbation is obtained subtracting a cubical fit, interpreted as the background wind, from the
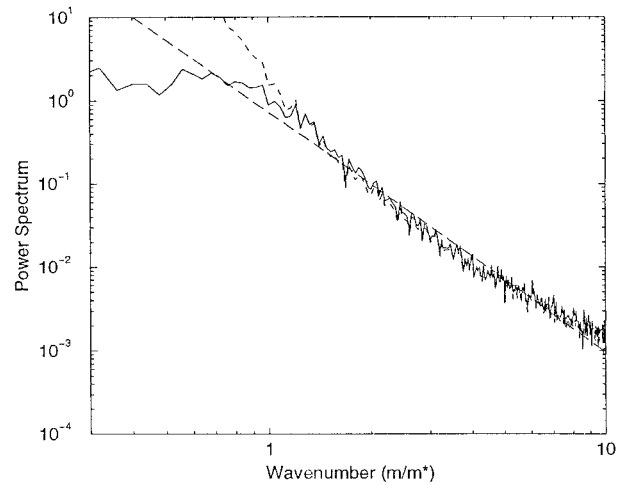

FIG. 3. Mean power spectrum for 30 profiles simulated with the model. The full line represents the mean of the Fourier transform calculated power spectra; the dashed line represents the mean of the approximations to every power spectrum with the series; and the straight line is the best fit to the power spectrum.

data (Eckermann et al. 1995). Then, applying a Bartlett window (Brigham 1974), contributions from the extremes of the interval are lowered. Figure 4 shows the resulting profile.

To identify discontinuity points, it is preferable to examine the derivative of the profile. A simple way to carry this out is to subtract the perturbation at successive points [i.e., $u(z_{i+1}) - u(z_i)$], which is shown in Fig. 5. In this figure several spikes suggest the presence of discontinuities. Being nonperiodic in nature, they will behave as true discontinuities from the point of view of the Fourier transform since they will result in a net leakage effect.
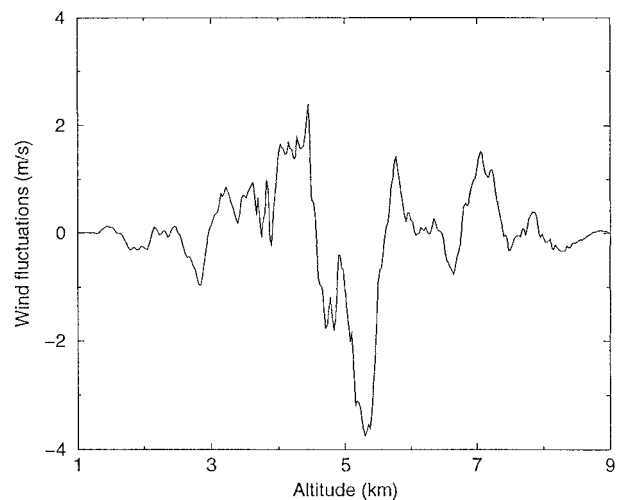

FIG. 4. Perturbation of a measured wind profile. The measurements used a drop sphere technique (Jimsphere) in Cape Kennedy on 16 April 1967. The perturbation has been multiplied by a Bartlett window.
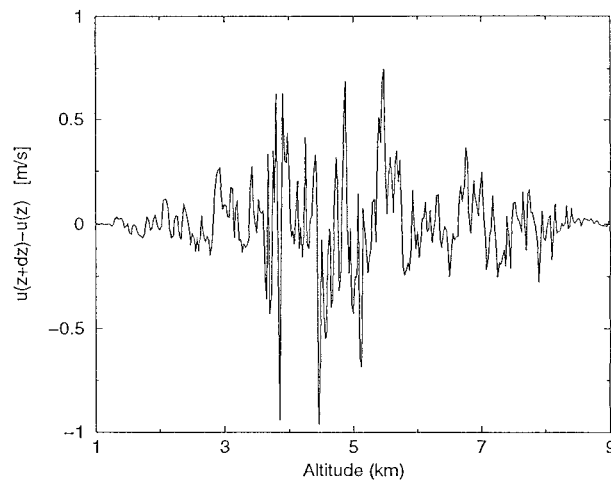
FIG. 5. Differences between successive points for the wind perturbation shown in Fig. 4. Notice the nonperiodic succession of jumps in the differential. Values of these jumps are within what can be considered normal.

FIG. 6. Function (5.1) for the harmonic corresponding to $m = 0.008$ cycles m^{-1} using the data shown in Fig. 4. A clear association between steps and jumps of Fig. 5 is observed. To help with the association, crosses mark the larger-jump positions.

The following integral function will be useful to analyze the contribution of the discontinuities to the Fourier coefficient:

$$C_n(z) = \frac{1}{\sqrt{L}} \int_{z_0}^{z} u(z) \cos(2\pi nz/L + \phi_n) \, dz, \quad (5.1)$$

where ϕ_n is the phase of the nth harmonic. Also note that from (3.1), $|C_n| = C_n(z_0 + L)$.

In Fig. 6 function (5.1) is plotted for the particular case of $m = 0.008$ cycles m^{-1}. The crosses on the abscissa axis represent the altitudes of the more prominent jumps. Clearly, the integral function (5.1) presents steps at the altitudes of these jumps, suggesting that the internal leakage is the dominant contribution to this mode amplitude.

In order to estimate the contribution of the spikes to the PS, we use Eq. (3.3) for $s = 0$ and taking only the 10 largest jumps. Figure 7 shows the so calculated PS together with the PS from the Fourier transform.

Notice that in the tail, both PS have similar energy content. Again, we suggest that the internal leakage created by nonperiodic jumps is dominant in the generation of the PS tail. The amplitude of the mode at hand is 1.05, while the approximation dominated by discontinuities gives 0.74. Also, the phase of this mode is dominated by the larger discontinuities with a value of 2.73, while 2.61 is the estimated one. Only when the superposition (3.3) is destructive, one notices increasingly important contributions from other points to the generation of the PS tail.

The analysis is independent of the quantitative values of the jumps, and the most important characteristic is their nonperiodicity. Even when the large jumps are somehow removed, there will be probably a larger number of smaller nonperiodic jumps taking over the leakage effect.
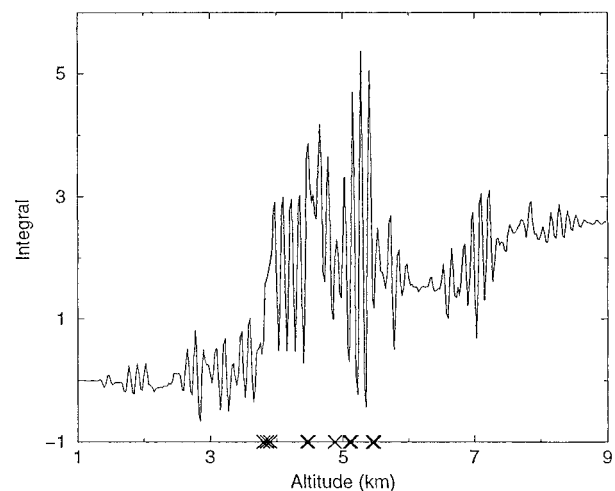
In other words, we would need a set of periodic jumps to avoid the appearance of internal leakage. This kind of periodicity has never been observed in actual profiles.

6. Discussion and conclusions

Every time wind profiles are Fourier transformed, there appears a spectrum different from the expected one; we can call this contamination in the sense that the energy content is spread and accumulation occurs at large wavenumbers. The latter, as we have shown, is a consequence of the lack of regularity, and the spreading results in a tail with slopes ranging from -2 to -4.
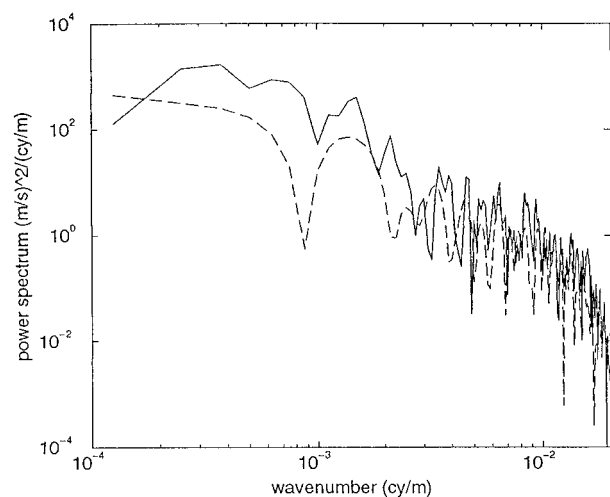

FIG. 7. The solid line represents the power spectrum for the profile of Fig. 4, and the dashed line the first-order estimation of the power spectrum obtained from the power series (3.4) using only the 10 largest jumps. Notice the similarities in both the slopes and energy content.

Undoubtedly, these effects are important in observed profiles, as seen above, and we would like to point out the need for a more systematic quantification of the energy due to the internal leakage in these profiles.

So far, the spectra from real profiles have been analyzed in terms of wave content in the profiles and therefore been thought in terms of physical processes. Our approach is different since we are analyzing the spectra as being the consequence of mathematical effects related to the Fourier transform. So, we find effects not related to waves that nevertheless generate amplitudes in the PS, and, what is very important, with slopes close to the observed ones.

The internal leakage is not only produced by the gravity wave termination but also by possible errors in the measurements as well as by isentropic advection of air parcels carried by the gravity wave field (Eckermann 1999). These processes generate amplitudes in the tail spectrum with slopes similar to the measured ones.

The expansion (3.4) takes into account processes such as changes in the wavelength and amplitude in the pre-breaking region—via the Taylor–Goldstein equation—which present internal leakage.

The prevailing models (Dewan and Good 1986) used to explain the PS tail are based on constant amplitude and wavelength across the interval. From Figs. 5 and 6, the high-wavenumber contributions come, in general, from very well defined height ranges, and therefore the terminating wave approaches are representative of these kind of effects.

REFERENCES

Allen, S. J., and R. A. Vincent, 1995: Gravity wave activity in the lower atmosphere: Seasonal and latitudinal variations. *J. Geophys. Res.,* **100,** 1327–1350.

Brigham, E. O., 1974: *The Fast Fourier Transform.* Prentice-Hall, 252 pp.

Chimonas, G., 1997: Waves and the middle atmosphere wind irregularities. *J. Atmos. Sci.,* **54,** 2115–2128.

Dewan, E. M., and R. E. Good, 1986: Saturation and the ''universal'' spectrum for vertical profiles of horizontal scalar winds in the atmosphere. *J. Geophys. Res.,* **91,** 2742–2748.

Eckermann, S. D., 1999: Isentropic advection by gravity waves: Quasi-universal M^{-3} vertical wavenumber spectra near the onset of instability. *Geophys. Res. Lett.,* **26,** 201–204.

——, I. Hirota, and W. K. Hocking, 1995: Gravity wave and equatorial wave morphology of the stratosphere derived from long-term rocket soundings. *Quart. J. Roy. Meteor. Soc.,* **121,** 149–186.

Endlich, R. M., R. C. Singleton, and J. W. Kaufman, 1969: Spectral analysis of detailed vertical wind speed profiles. *J. Atmos. Sci.,* **26,** 1030–1041.

Erdélyi, A., 1956: *Asymptotic Expansions.* Dover, 107 pp.

Fritts, D. C., 1984: Gravity wave saturation in the middle atmosphere: A review of theory and observations. *Rev. Geophys.,* **22,** 275–308.

Hines, C. O., 1991: The saturation of gravity waves in the middle atmosphere. Part II: Development of Doppler-spread theory. *J. Atmos. Sci.,* **48,** 1360–1379.

Hodges, R. R., Jr., 1967: Generation of turbulence in the upper atmosphere by internal waves. *J. Geophys. Res.,* **72,** 3455–3458.

Press, W. H., S. A. Teukolsky, W. T. Vetterling, and B. P. Flannery, 1992: *Numerical Recipes in FORTRAN.* 2d ed. Cambridge University Press, 964 pp.

Sato, K., and M. Yamada, 1994: Vertical structure of atmospheric gravity waves revealed by the wavelet analysis. *J. Geophys. Res.,* **99,** 20 623–20 631.

Teitelbaum, H., and C. Sidi, 1979: Discontinuity formation due to gravity wave propagation in a shear layer. *Phys. Fluids,* **22,** 209–213.

VanZandt, T. E., 1982: A universal spectrum of buoyancy waves in the atmosphere. *Geophys. Res. Lett.,* **9,** 575–578.

Weinstock, J., 1990: Satured and unsaturated spectra of gravity waves and scale-dependent diffusion. *J. Atmos. Sci.,* **47,** 2211–2225.